HHMI Author Manuscript

HHMI Author Manuscript

HHMI Author Manuscript

Published as: *Nat Neurosci*. 2009 October ; 12(10): 1257–1265.

Presynaptic CaV2 calcium channel traffic requires CALF-1 and the alpha2-delta subunit UNC-36

Yasunori Saheki and **Cornelia I. Bargmann**
Howard Hughes Medical Institute and Laboratory of Neural Circuits and Behavior, The Rockefeller University, New York, NY 10065, USA

Abstract

Presynaptic voltage-gated calcium channels provide calcium for synaptic vesicle exocytosis. We show here that a GFP-tagged alpha1 subunit of the *C. elegans* CaV2 channel, UNC-2, is localized to presynaptic active zones of sensory and motor neurons. Synaptic localization of CaV2 requires the alpha2-delta subunit UNC-36 and CALF-1 (Calcium Channel Localization Factor-1), a neuronal transmembrane protein that localizes to the endoplasmic reticulum. In *calf-1* mutants, UNC-2 is retained in the endoplasmic reticulum but other active zone components and synaptic vesicles are delivered to synapses. Acute induction of *calf-1* mobilizes preexisting UNC-2 for delivery to synapses, consistent with a direct trafficking role. The alpha2-delta subunit UNC-36 is also required for endoplasmic reticulum exit of UNC-2, but has additional functions. Genetic and cell biological interactions suggest that CALF-1 couples intracellular traffic to functional maturation of CaV2 presynaptic calcium channels.

Introduction

Neuronal voltage-gated calcium channels (VGCCs) are central regulators of synaptic vesicle exocytosis, dendritic integration, and calcium-dependent gene regulation 1. A VGCC consists of one pore-forming alpha1 subunit that defines intrinsic channel properties, and auxiliary alpha2-delta, beta and sometimes gamma subunits that modify channel kinetics and channel density 2. Specific genes in the CaV gene family encode physiologically distinct alpha1 subunits. Mammalian L-type channels with CaV1 alpha1 subunits are mainly required for gene regulation and dendritic integration, N-, P/Q- and R-type channels with CaV2 alpha1 subunits are required for neurotransmitter release and dendritic calcium transients, and T-type channels with CaV3 alpha1 subunits are required for repetitive firing 1. Disruptions of VGCC function are implicated in human epilepsy, migraine, autism-spectrum disorders, and bipolar disease, underlining the importance of these channels in the regulation of neuronal excitability and function3.

Users may view, print, copy, and download text and data-mine the content in such documents, for the purposes of academic research, subject always to the full Conditions of use:http://www.nature.com/authors/editorial_policies/license.html#terms

TEL: 212-327-7241; FAX: 212-327-7243; e-mail: cori@rockefeller.edu.

Author contributions
Y.S. and C.I.B. designed the project, and Y.S. conducted the experiments. Y.S. and C.I.B. wrote the paper.

HHMI Author Manuscript HHMI Author Manuscript HHMI Author Manuscript

CaV1, CaV2, and CaV3-related genes are found in invertebrates as well as vertebrates 4. The fruit fly *Drosophila melanogaster* and the nematode *Caenorhabditis elegans* each have one predicted CaV2 alpha1 subunit, encoded by the *cacophony* and *unc-2* genes, respectively. Fly CaV2/*cacophony* mutants are inviable, with defects in calcium-dependent neurotransmitter release at the neuromuscular junction suggesting the loss of the presynaptic calcium current 5, 6. A GFP-tagged Cacophony protein is localized to presynaptic active zones, consistent with a role at synapses 7. *C. elegans* CaV2/*unc-2* mutants are uncoordinated, with defects in evoked neurotransmitter release at the neuromuscular junction 8–10. These phenotypes suggest a conserved role for CaV2 channels as presynaptic regulators of synaptic transmission.

The surface expression and localization of presynaptic VGCCs can be affected by channel subunit composition and by other proteins. The alpha2-delta auxiliary subunit increases channel activity and plasma membrane expression of mammalian CaV2 alpha1 subunits 11, and increases synaptic expression and activity of *Drosophila* Cacophony/CaV2 protein 12, 13. The beta auxiliary subunit increases plasma membrane expression of multiple mammalian VGCC classes 14, 15. Other proteins that regulate presynaptic VGCC localization *in vivo* include the *Drosophila* active zone protein Bruchpilot/ELKS 16, the *Drosophila* eight-transmembrane domain protein Fuseless 17, and the vertebrate extracellular matrix protein laminin beta2 18. Many additional candidate regulators of presynaptic VGCCs have been studied in cultured cells, including scaffolding proteins such as CASK, Mint and Veli 19, and the dynein light chain protein Tctex1 20.

To complement studies of VGCCs in cultured cells, and to explore CaV2 channel traffic *in vivo*, we here analyze neuronal calcium channel localization and function in *C. elegans*. The *C. elegans* genome encodes three predicted VGCC alpha1 subunits, *egl-19* (CaV1), *unc-2* (CaV2), and *cca-1* (CaV3) 4. UNC-2 is a candidate presynaptic voltage-gated calcium channel based on its sequence similarity to CaV2 channels, neuronal expression, and synaptic transmission defects. We show that a functional GFP-tagged UNC-2 is concentrated at presynaptic active zones of sensory neurons and motor neurons. UNC-2 localization requires the alpha2-delta subunit UNC-36 and a newly-described endoplasmic reticulum protein, CALF-1 *(Calcium Channel Localization Factor-1)*. CALF-1 and UNC-36 have partly overlapping activities in the traffic and functional maturation of UNC-2 channels.

Results

The CaV2 alpha1 subunit UNC-2 localizes to presynaptic active zones

A full-length, GFP-tagged *unc*-2 cDNA rescued the uncoordinated movement of *unc-2* mutants when expressed from a pan-neuronal promoter (see Methods). To examine its subcellular localization, GFP::UNC-2 was expressed under cell type-specific promoters together with the synaptic vesicle marker RAB-3::mCherry (hereafter, RAB-3)21. When expressed in AWC olfactory neurons, GFP::UNC-2 localized to axonal puncta that overlapped with RAB-3, consistent with presynaptic localization (Fig. 1a–g). GFP::UNC-2 was also present in the cell body, but was excluded from the dendrite, cilia, and nucleus. When expressed in VD and DD GABAergic motor neurons, GFP::UNC-2 localized with

HHMI Author Manuscript HHMI Author Manuscript HHMI Author Manuscript

RAB-3 in the ventral and dorsal nerve cords (Fig. 1h–j). When expressed in the DA9 cholinergic motor neuron, GFP::UNC-2 localized with RAB-3 in the dorsal presynaptic region of the axon (Fig. 1k–n). In each case, the GFP::UNC-2 protein was present in the cell body, but largely excluded from dendrites and asynaptic regions of axons.

Presynaptic calcium channels function at active zones, the plasma membrane sites of synaptic vesicle secretion. GFP::UNC-2 puncta were often more focal than RAB-3 puncta (Fig. 1), suggesting that UNC-2 might localize to active zones. In agreement with this idea, GFP::UNC-2 in AWC axons colocalized closely with the active zone markers ELKS-1::mCherry and SYD-2::mCherry (Fig. 1d–f, Supplementary Fig. 1a–c).

To define genes required for UNC-2 localization to synapses, we first examined candidate mutants using GFP::UNC-2 and RAB-3 expressed in AWC. Synaptic vesicle clustering and active zone structure in *C. elegans* are regulated by SAD-1 kinase, SYD-2/liprin-alpha, SYD-1 and RPM-1/Hiw/Esrom/PAM 22–25. In all of these mutants, GFP::UNC-2 puncta associated with RAB-3 in AWC axons, although there were defects in the spacing, size, and number of clusters (Supplementary Fig. 2a–d). Several other candidate genes had no obvious effect on GFP::UNC-2 localization in AWC: *elks-1*, the *C. elegans* homolog of *Drosophila bruchpilot* 16, *nrx-1*, the sole *C. elegans* neurexin homolog, *lin-2/CASK*, *lin-7/Veli*, and *lin-10/MINT* PDZ proteins of the tripartite complex, or the synaptic exocytosis and endocytosis mutants *unc-13*, *unc-10/RIM*, *dpy-23/AP2*, *unc-101/AP1*, *unc-11/AP180*, and *unc-31/CAPS* (Supplementary Fig. 2e–o). A mutation in the KIF1A kinesin gene *unc-104* caused RAB-3 to disappear from AWC axons, consistent with the known requirement for KIF1A in synaptic vesicle traffic 26, but GFP::UNC-2 puncta were present and apparently normal in *unc-104* mutants (Supplementary Fig. 2p). Similarly, a partial loss of function mutation in the KIF5 kinesin heavy chain gene *unc-116* affected RAB-3 localization, but maintained GFP::UNC-2 colocalization with RAB-3 (Supplementary Fig. 2q). The absence of obvious GFP::UNC-2 phenotypes in these mutants does not exclude subtle functions, redundant functions, or functions in other classes of neurons.

unc-36 alpha2-delta mutants have uncoordinated phenotypes and other neuronal phenotypes similar to those of *unc-2* mutants 10, 27, 28. GFP::UNC-2 was barely detectable in the AWC axons of a null *unc-36* mutant, but was still detectable in the cell body, demonstrating a requirement for UNC-36 in the sorting, folding, or localization of UNC-2 *in vivo* (Supplementary Fig. 2r). RAB-3 puncta were normal, suggesting that synaptic vesicle clustering was unaffected.

UNC-2 synaptic puncta are reduced in *calf-1* mutants

A genetic screen for mutants with altered GFP::UNC-2 expression in AWC yielded three mutants with few axonal GFP::UNC-2 puncta, but apparently normal RAB-3 puncta (see Methods). Two mutants had an uncoordinated phenotype and failed to complement the alpha2-delta subunit mutant *unc-36(e251)*, suggesting that they are mutant for *unc-36*. The third mutant affected a new gene, here named *calf-1(ky867)* or Calcium channel Localization Factor-1. In *calf-1(ky867)* mutants, GFP::UNC-2 was nearly undetectable in AWC axons, but the synaptic vesicle marker RAB-3 (Fig. 2a–c) and the active zone markers ELKS-1 (Fig. 2d–f) and SYD-2 (Supplementary Fig. 1d–f) appeared normal. The total

HHMI Author Manuscript

HHMI Author Manuscript

HHMI Author Manuscript

fluorescence intensity of axonal GFP::UNC-2 as well as the number of puncta per axon were greatly reduced, whereas GFP::UNC-2 fluorescence in the cell body was slightly increased (Fig. 2g,h); minimal effects were detected upon similar quantification of RAB-3 (Fig. 2g,h). These results suggest that *calf-1* mutants have a selective defect in presynaptic calcium channel localization.

calf-1 also affected GFP::UNC-2 localization in motor neurons. The dorsal nerve cord of *calf-1* mutants had reduced levels of GFP::UNC-2 fluorescence and few GFP::UNC-2 puncta, but near-normal RAB-3 puncta, suggesting a loss of UNC-2 from DD synapses (Fig. 2i–l). In the ventral nerve cord, some GFP::UNC-2 puncta were visible, but these puncta did not localize with RAB-3 at VD synapses (Fig. 2j). Consistent with a defect in motor neurons, *calf-1* mutants had a distorted sinusoidal posture and moved very slowly on agar surfaces or in liquid, like *unc-2* mutants (Fig. 2m and data not shown).

In *calf-1* mutants, the GFP::UNC-2 signal in AWC cell bodies overlapped with the endoplasmic reticulum marker CP450::mCherry 29, suggesting that GFP::UNC-2 was retained in the endoplasmic reticulum (Supplementary Fig. 3a–c). Support for this conclusion came from examining GFP::UNC-2 in ventral cord processes of VD and DD neurons. In wild-type animals, GFP::UNC-2 in ventral cord processes was largely separated from the endoplasmic reticulum marker CP450::mCherry, but in *calf-1* mutants, GFP::UNC-2 and CP450::mCherry overlapped extensively (Supplementary Fig. 3d–i). These results suggest that GFP::UNC-2 preferentially accumulates in endoplasmic reticulum or related components in *calf-1* mutants.

The functional consequences of *unc-2* and *calf-1* mutations were examined by calcium imaging of AWC sensory neurons and AIB interneurons, which are postsynaptic targets of AWC. AWC calcium levels reported by the fluorescent indicator G-CaMP fall slightly upon addition of the attractive odor isoamyl alcohol, and rise upon odor removal; similar signals are subsequently observed in AIB interneurons 30. In *unc-2* and *calf-1* mutants, the AWC sensory responses to odors were of normal magnitude (Supplementary Figure 4), but postsynaptic AIB responses to odor removal were reduced (Figure 2n). Approximately half of the *unc-2* and one third of *calf-1* AIB neurons did not respond to odor removal, although those AIB neurons that did respond had similar response magnitudes to wild type (Figure 2o). These results suggest that *unc-2* and *calf-1* affect neuronal signaling between AWC and AIB neurons in similar ways, reducing but not eliminating synaptic communication (see Discussion).

calf-1 encodes a neuronal transmembrane endoplasmic reticulum protein

Genetic mapping and transgenic rescue identified *calf-1* as the predicted gene B0250.2 (Fig. 3, Methods and Supplementary Fig. 3j). Sequencing of *calf-1(ky867)* DNA revealed a C to T mutation resulting in an early stop codon in the B0250.2 open reading frame. The *calf-1* mutant is fully recessive, and a *calf-1* gene with the *ky867* mutation did not affect GFP::UNC-2 localization or locomotion when injected into wild-type animals (data not shown). These results suggest that *ky867* is a loss of function allele of *calf-1*/B0250.2.

HHMI Author Manuscript

HHMI Author Manuscript

HHMI Author Manuscript

calf-1 encodes a predicted type I transmembrane protein with a hydrophobic membrane-spanning region, a highly basic region, and a proline-rich region (Fig. 3a). The region C-terminal to the transmembrane domain is predicted to be cytosolic. Homologs of *calf-1* were identified in other nematode species (Fig. 3b), but not in other organisms. Among nematodes, conservation of CALF-1 was highest in the predicted transmembrane domain and the adjacent basic region (Fig. 3c).

The uncoordinated phenotype and defective GFP::UNC-2 localization in *calf-1* mutants were rescued by a 0.5 kb *calf-1* cDNA expressed under 0.8 kb of *calf-1* upstream sequence (Fig. 4a,b). When the same 0.8 kb promoter was used to drive expression of GFP, fluorescence was detected in many or all neurons, but not in other tissues (Fig. 4c,d). Coexpression with an *odr-1::mCherry* transgene confirmed that the *calf-1* promoter drove expression in AWC neurons (Fig. 4e–g).

Expression of the *calf-1* cDNA under the control of the pan-neuronal *tag-168* promoter rescued the GFP::UNC-2 localization phenotypes and locomotory behavior of *calf-1* mutants, but expression from the muscle-specific *myo-3* promoter did not (Fig. 4a, b). Expression of *calf-1* under the AWC-selective *odr-3* promoter rescued GFP::UNC-2 localization in AWC neurons, and expression of *calf-1* under the VD/DD motor neuron promoter *unc-25* rescued dorsal GFP::UNC-2 localization in DD neurons (Fig. 4h,i). These results suggest that *calf-1* acts cell autonomously to localize UNC-2.

A *calf-1* cDNA that was tagged with GFP fully rescued the locomotion defects in *calf-1* mutants (see Methods). When expressed in AWC neurons, CALF-1::GFP was exclusively localized to the cell body, and not to axons or synapses (Fig. 4j–l). The CALF-1::GFP signal overlapped extensively with mCherry-labeled endoplasmic reticulum markers CP450, cb5, and RAMP4 (Fig. 4m–o, Supplementary Fig. 5a–f) but not with the Golgi marker ManII::mCherry (Fig. 4p–r). When expressed in VD and DD motor neurons, CALF-1::GFP was present in cell bodies and in a few puncta in ventral processes; these puncta did not overlap with RAB-3 or the Golgi marker, but did overlap with an endoplasmic reticulum marker (Supplementary Fig. 5g–r). These results suggest that CALF-1 is a neuron-specific endoplasmic reticulum protein.

Functional motifs within CALF-1 promote endoplasmic reticulum retention

To identify sequences necessary for CALF-1 function, we tested mutant proteins for their ability to rescue either GFP::UNC-2 clusters in AWC or coordinated locomotion. Deletion of the CALF-1 transmembrane domain or replacement with the integrin PAT-3 transmembrane domain eliminated its activity (Fig. 5a). CALF-1 was active following individual deletion of three other regions, the basic region (deletion I), the proline-rich region (deletion II), or the C-terminal region (deletion III). Simultaneous deletion of all three regions inactivated CALF-1, but inclusion of either the basic region, or the proline-rich and C-terminal regions together, was sufficient for rescue (deletion I–VI).

Any of the three regions of CALF-1 that promote its function -- the transmembrane domain, the basic region, and the combined proline-rich and C-terminal region -- was sufficient to cause endoplasmic reticulum retention of a GFP-tagged protein in intestinal cells (Fig. 5b

HHMI Author Manuscript

HHMI Author Manuscript

HHMI Author Manuscript

and Methods). Embedded in the basic region and C-terminal region of CALF-1 are multiple arginine-x-arginine (RXR) motifs (Fig. 3c), which can function as endoplasmic reticulum retention motifs in other transmembrane proteins 31. A C-terminal truncation of CALF-1 that removed RQR and RKR motifs was competent for rescue (RKR deletion), but a larger C-terminal deletion that eliminated RQR, RKR, RAR, and RLR motifs inactivated CALF-1 (RLRE deletion) (Supplementary Fig. 6a–c). Interestingly, a small fusion protein consisting of the CALF-1 transmembrane domain and a 16 amino acid arginine-rich endoplasmic reticulum retention motif from the G-protein coupled alpha2 adrenergic receptor 32 partly rescued *calf-1* mutants (Supplementary Fig. 6a,b); similar fusions of the CALF-1 transmembrane domain to KDEL or KKYL endoplasmic reticulum retention motifs were inactive. These results suggest that arginine-rich endoplasmic reticulum retention motifs contribute to *calf-1* activity.

unc-36 affects UNC-2 maturation and function

To gain further insight into the relationships between *unc-2*, *calf-1*, and *unc-36*, we examined multiple phenotypes and genetic interactions in these mutants. Both canonical null *unc-36* mutations and new *unc-36* mutations from our screen caused defects in GFP::UNC-2 localization that resembled those of *calf-1* mutants: GFP::UNC-2 was absent from AWC axons and dorsal VD and DD processes, but synaptic RAB-3 localization appeared normal (Fig. 6a–d). In the ventral nerve cord, GFP::UNC-2 in VD/DD neurons rarely overlapped with the synaptic vesicle marker RAB-3 (Fig. 6e) but overlapped extensively with the endoplasmic reticulum marker CP450 (Fig. 6f). These observations suggest that *unc-36* mutations cause GFP::UNC-2 to accumulate in the endoplasmic reticulum. In agreement with this hypothesis, *unc-36* mutants had increased accumulation of GFP::UNC-2 in the AWC cell body and perinuclear region compared to wild type, although the effect was less marked than in *calf-1* mutants (Supplementary Fig. 7a–d).

A biologically active, GFP-tagged UNC-36 protein was localized both to the plasma membrane and to internal membranes of neurons, suggesting that it could function either in the endoplasmic reticulum with CALF-1, or in the synapse with UNC-2, or at both locations (Fig. 6g). In AWC neurons, UNC-36::GFP was largely perinuclear, and overlapped with the endoplasmic reticulum marker CP450 (Supplementary Fig. 7e–g); unlike GFP::UNC-2, it was not concentrated at AWC synapses. Perinuclear UNC-36::GFP localization in AWC was unchanged in *calf-1* mutants; similarly, CALF-1::GFP localization in AWC, VD, and DD was unchanged in *unc-2* and *unc-36* mutants (Supplementary Fig. 7h–v).

Genetic interactions were consistent with related functions of *calf-1*, *unc-36*, and *unc-2*. All three mutants and all double mutants were slow-moving but not paralyzed, with similar phenotypes (Fig. 6h). Overexpression of untagged UNC-2 from a pan-neuronal promoter significantly improved the *calf-1* locomotion phenotype (Fig. 6h). This result suggests that the locomotion defect in *calf-1* is related to reduced *unc-2* activity, and supports a primary role for *calf-1* as a cofactor for *unc-2*.

Overexpression of *calf-1* from a pan-neuronal promoter rescued synaptic GFP::UNC-2 puncta in *unc-36* mutants, an effect that was weak in AWC and robust in VD and DD (Fig. 6i–k). However, *calf-1* overexpression did not rescue the locomotion defects of *unc-36*

HHMI Author Manuscript

HHMI Author Manuscript

HHMI Author Manuscript

mutants (Fig. 6h), suggesting that *unc-36* mutants are defective in locomotion even when some UNC-2 is delivered to synapses. *unc-36* overexpression did not rescue GFP::UNC-2 localization or locomotion defects in *calf-1* mutants (Fig. 6h–j).

calf-1, *unc-2*, and *unc-36* also function together in a calcium-dependent developmental pathway that generates asymmetric gene expression patterns in the left and right AWC neurons 33. Left-right asymmetry is disrupted in about 50% of *unc-2* mutants, an effect that is enhanced in *unc-2 egl-19*/CaV1 double mutants 28. As *unc-36* mutations affect both CaV1 and CaV2 channels, *unc-36* has a stronger defect than *unc-22*8. *calf-1* mutants had defects in AWC gene expression that closely resembled those of *unc-2* null mutants, and an *unc-2 calf-1* double mutant was similar to the single mutants (Supplementary Table 1). These results suggest that the *calf-1* mutation specifically affects *unc-2* function in AWC, and not the genetically separable activities of *unc-36* and *egl-19* in the same cell.

CALF-1 acts acutely to deliver UNC-2 to synapses

The genetic analysis of *calf-1* suggests that UNC-2 accumulates in endoplasmic reticulum until CALF-1 allows its exit, but do not demonstrate a direct mobilization of UNC-2. To examine the acute effects of *calf-1*, we used the heat shock promoter *hsp16.2* 34 to drive expression of *calf-1* under temperature control. A three hour heat pulse in adult animals was sufficient to rescue synaptic GFP::UNC-2 localization in AWC neurons, and also restored coordinated locomotion to *calf-1* mutants (Fig. 7a–c). The adult rescue of *calf-1* mutants argues for a role of CALF-1 in ongoing delivery of UNC-2 to synapses, and against an essential role in synaptic development.

The rapid action of *calf-1* after heat shock made it possible to examine effects of *calf-1* on the dynamic behavior of UNC-2 protein. A pulse-chase protocol was designed to test the mobilization hypothesis directly, using *hs::calf-1* and a fluorescently labeled pool of UNC-2 protein (Fig. 7d). UNC-2 was tagged at its N-terminus with the photoconvertible protein Dendra2, which irreversibly changes from green to red emission upon UV irradiation 35. Dendra2::UNC-2 protein behaved similarly to GFP::UNC-2, both before and after photoconversion; it had a synaptic location in wild-type animals, but accumulated in cell bodies of *calf-1* mutants (data not shown). In the pulse-chase experiment, a pool of Dendra2::UNC-2 protein in the cell bodies of the tail was photoconverted to red in *calf-1; hs::calf-1* animals raised at low temperatures. After photoconversion, these animals were subjected to a heat shock to induce *calf-1* expression (Fig. 7d,e). In 7 of 9 animals subjected to heat shock, red Dendra2::UNC-2 was mobilized from the cell bodies to puncta within the nerve ring, where many tail neurons form synapses (Fig. 7f). No red Dendra2::UNC-2 puncta were found in the nerve ring in the absence of heat shock (Fig 7f, n=9 animals). These results demonstrate that UNC-2 within the cell body, most likely the endoplasmic reticulum, is acutely mobilized by CALF-1. In agreement with this conclusion, the heat shock protocol significantly reduced the amount of red Dendra2::UNC-2 in the cell body while increasing its levels at synapses (Fig. 7g).

HHMI Author Manuscript HHMI Author Manuscript HHMI Author Manuscript

Discussion

Calcium channels in *C. elegans*, like their homologs in other animals, have distinctive functions and subcellular locations. We found that the UNC-2/CaV2 protein is highly enriched in presynaptic puncta, where it may provide calcium for exocytosis 8–10. Signaling from AWC neurons to postsynaptic AIB neurons is reduced but not eliminated in *unc-2* mutants, indicating that UNC-2 cannot be the only source of presynaptic calcium in AWC. These observations were made by *in vivo* calcium imaging, a relatively low-resolution method, so they do not provide detailed information about synaptic mechanisms. However, the general conclusions are consistent with electrophysiological studies at the *C. elegans* neuromuscular junction showing that *unc-2* mutants have reduced synaptic release, but retain residual synaptic function (ref. 9 and J. Madison and J. Kaplan, personal communication). The axonal NCA channels are attractive candidates for a second presynaptic activity, since these mutants have variable failures in presynaptic calcium signals that are reminiscent of the variable failures in *unc-2* mutants36. EGL-19/CaV1 channels are also candidates; although EGL-19 is expressed mainly in the cell body (Y.S., unpublished results), inhibitory interactions between EGL-19 and UNC-2 may allow EGL-19-dependent compensation in *unc-2* mutants 28. Homeostatic compensation may also upregulate postsynaptic glutamate receptors to potentiate the AIB response 37.

Efficient exit of a GFP-tagged UNC-2 from the endoplasmic reticulum requires both the alpha2-delta subunit UNC-36 and the endoplasmic reticulum protein CALF-1. Proteins that promote the surface expression of channels can be divided into two categories: auxiliary subunits and regulators of biogenesis 38. Auxiliary proteins like TARPs (for glutamate receptors) and MinK (for potassium channels) first associate with the channel in the endoplasmic reticulum, but remain associated at the plasma membrane where they modify channel properties. Their function may be primarily channel modulation, and secondarily channel traffic. Our results suggest that the alpha2-delta subunit UNC-36 acts as an auxiliary subunit that regulates both UNC-2 exit from the endoplasmic reticulum and UNC-2 function (Supplementary Fig. 7w).

Alpha2-delta subunits in other animals are also implicated in CaV2 traffic. *Drosophila straightjacket* alpha2-delta mutants have a major defect in synaptic transmission, and a minor decrease in CaV2 channel levels at the synapse (25–40%) 12, 13. Similarly mammalian alpha2-delta subunits can affect both CaV2 traffic and function; mammalian alpha2-delta-1 and alpha2-delta-2 are the primary targets of the antiepilepsy drug gabapentin, which reduces surface expression of CaV2 channels in cultured neurons and heterologous cells 11, 39. The precise trafficking step affected by *straightjacket* and mammalian alpha2-delta subunits has not been defined, but our results indicate that one effect of UNC-36 on UNC-2 occurs during exit from the endoplasmic reticulum. Mammalian and fly alpha2-delta mutants appear to have a milder trafficking defect than *unc-36*, perhaps because of redundancy among alpha2-delta genes: *Drosophila* has three predicted genes encoding alpha2-delta subunits, and mammals have four, but *C. elegans* has only two (*unc-36* and the uncharacterized gene *tag-180).* However, the interpretation of our experiments and those in *Drosophila* is limited by the fact that localization was only

HHMI Author Manuscript HHMI Author Manuscript HHMI Author Manuscript

examined using overexpressed GFP-tagged CaV2 proteins, which could have different sorting requirements from native CaV2 channels.

CALF-1 appears to function primarily in UNC-2 biogenesis, not as an auxiliary subunit (Supplementary Fig. 7w). CALF-1 resides in the endoplasmic reticulum, and CALF-1::GFP is not detectable at synapses, whereas synaptic GFP::UNC-2 is easily detected. Thus if CALF-1 remains associated with UNC-2 at the cell surface, that association is transient or sub-stoichiometric. *calf-1* acts rapidly and cell-autonomously to affect UNC-2 localization, apparently by ongoing regulation of UNC-2 exit from the endoplasmic reticulum. This activity is consistent with a role as cargo-specific chaperone, or “outfitter”, for UNC-2 40. Among the overlapping functions of cargo-specific chaperones are protein folding activities, prevention of aggregation and retrotranslocation of transmembrane proteins from the endoplasmic reticulum into the cytosol, and recruitment of COPII vesicle proteins for endoplasmic reticulum exit 41–43.

CALF-1 contains multiple RXR motifs, sequences that were first identified for their ability to retain unfolded or partially assembled potassium channels in the endoplasmic reticulum 31, 32. *Cis*-acting RXR motifs regulate sorting of Kir and Kv potassium channels, cystic fibrosis-associated CFTR channels, NMDA-type glutamate receptors, cardiac sodium channels, and GABA-B receptors 43. Unlike other endoplasmic reticulum retention motifs such as KDEL, RXR motifs can stimulate endoplasmic reticulum exit in some contexts, particularly when multimerized or when bound by 14-3-3 proteins 43. CALF-1 contains many RXR motifs, but acts in *trans* to UNC-2 and not in *cis*. In its small size, transmembrane structure, and proposed function, it resembles the RXR-containing invariant chain that regulates MHC Class II traffic through internal membranes 44.

We suggest that CALF-1 acts at an assembly or endoplasmic reticulum exit checkpoint for UNC-2, perhaps by recruiting coat proteins or releasing UNC-2 from endoplasmic reticulum retention factors (Supplementary Fig. 7w). CALF-1-dependent endoplasmic reticulum exit normally occurs after UNC-2 and UNC-36 interact, but can occur under other circumstances when UNC-2 or CALF-1 is overexpressed. Conserved CALF-1 homologs are only recognizable in nematodes, but more distantly-related proteins in other species could have analogous activities. For example, the poorly-understood gamma subunits of mammalian calcium channels have multiple RXR motifs and multiple prolines in their C-terminal cytoplasmic domains, like CALF-1. Defining the conserved, species-specific, and cell type-specific components of presynaptic CaV2 localization is a challenge for further experiments.

Methods

Strains

Wild-type worms were Bristol variety N2. Strains were maintained using standard methods at 21–23° C. Some strains were provided by the *Caenorhabditis* Genetics Center and the National Bioresource Project. Mutants used were *calf-1(ky867), unc-2(lj1), unc-36(e251), syd-2(ju37), sad-1(ky289), rpm-1(js410), syd-1(ju82), elks-1(tm1233), nrx-1(ds1), lin-2(n1610), lin-7(n308cs), lin-10(e1439), unc-13(e51), unc-10(e102), dpy-23(e840), unc-101(m1), unc-11(ky280), unc-31(e928), unc-104(e1265), unc-116(e2310)*.

HHMI Author Manuscript HHMI Author Manuscript HHMI Author Manuscript

Germline transformation was carried out as described 34. *odr-3::GFP::unc-2*, *tag-168::Dendra2::unc-2* and *unc-25::GFP::unc-2* were injected at 100 ng/μl. For rescue, overexpression and structure-function analysis, all *calf-1* plasmids were injected at 20 ng/μl except *hsp16.2::calf-1* at 10 ng/μl. Relatively high levels of GFP::UNC-2 and Dendra2::UNC-2 were needed for reliable visualization, and these overexpressed, tagged proteins might distort endogenous traffic. However, GFP::UNC-2 and Dendra2::UNC-2 were able to rescue *unc-2*-dependent locomotion, and were reliably trafficked to synapses in heat-shocked *calf-1* animals carrying *hsp16.2::calf-1*, indicating that the proteins in transgenic animals can interact effectively with the trafficking machinery.

For localization experiments, *calf-1::GFP* fusion plasmids were injected at 10 ng/μl. *unc-36::GFP* fusion plasmids were injected at 50ng/μl. All cell compartment markers including *odr-3::mCherry::rab-3* and *odr-3::CP450::mCherry* were injected at 0.5 to 5ng/μl. *ofm-1::GFP, ofm-1::DsRed, elt-2::mCherry, odr-1::mCherry, odr-1::DsRed, odr-1::GFP and flp-17::mCherry* were used as coinjection marker and injected at 6–20 ng/μl.

A complete list of transgenes and strains is included in Supplementary Information.

Isolation and characterization of *calf-1(ky867)*

A strain expressing GFP::UNC-2 in AWC *(kyIs442)* was mutagenized with EMS according to standard protocols 45. 209 F1s were cloned into different plates, and 30 to 50 F2 animals from individual F1 animals were subjected to a direct visual screen under a compound microscope. The mutants were isolated based on the loss of GFP::UNC-2 puncta from the AWC axon as observed with a Plan Apochromat 63x objective on a Zeiss Axioplan2 microscope.

Mapping and cloning of *calf-1*

calf-1(ky867) was mapped to the far right end of LGV using SNP polymorphisms in the CB4856 strain 46. A genomic fragment containing only the B0250.2 reading frame with 0.8 kb of 5′ sequence and 1.2 kb of 3′ sequence was generated by PCR and injected at 1 ng/μl into *calf-1(ky867)* mutants. The PCR fragment rescued both uncoordinated movements and GFP::UNC-2 localization in AWC axons. To identify the *calf-1* mutation, the *calf-1* genomic coding region in *ky867* was amplified by PCR, and PCR products were sequenced.

Molecular biology

Standard molecular biology techniques were used. Details of plasmid construction and primers are in Supplementary Information.

Fluorescence microscopy and quantification

Animals were mounted on 4% agarose pads containing 400μM tetramisole. Multiple transgenic lines of each transgene were examined for fluorescent expression and localization patterns. Wide-field fluorescence images were obtained on Zeiss Axioplan2 imaging system (Fig. 1a–f, h,i, k–m; Fig. 2a–f, i,j; Fig. 4c,d; Fig. 6a–f, k; Fig. 7e,f; Supplementary Fig. 1a–f; Supplementary Fig. 2a–r; Supplementary Fig. 3a–i). Confocal images were obtained on

HHMI Author Manuscript HHMI Author Manuscript HHMI Author Manuscript

Zeiss LSM 510 META laser scanning confocal imaging system (Fig. 4e–g, j–r; Fig. 5b bottom panels; Fig. 6g; Supplementary Fig. 5a–r; Supplementary Fig. 7a–c, e–v).

To quantify fluorescence intensities and number of fluorescent clusters, images were captured under consistent detector settings with a Hamamatsu Photonics C2400 CCD camera on a Zeiss Axioplan2 Imaging System with a 63x Plan-Apochromat objective and Metamorph software. ImageJ (NIH) was used to quantify fluorescence in AWC axons and cell bodies and DD dorsal axons. Images of AWC nerve rings and cell bodies were projected into a single plane by maximum projection; for DD, a single image of best focus was chosen for the quantification. Background intensity was subtracted and fluorescent clusters containing signals above an arbitrary threshold were measured for the total fluorescence intensity and the number of fluorescent clusters. The same thresholds were used for all images in each quantification. Normalized fluorescence intensity was obtained by dividing individual values with mean total fluorescence intensity of wild-type control animals. For the perinuclear region of AWC, a single image of best focus was chosen for the quantification and maximum fluorescence intensity was measured after background subtraction (Supplementary Fig. 7d). 6–10 animals were scored for each experiment.

Calcium imaging

Calcium imaging was performed as described 30. For AWC^{ON} imaging, the strain CX10536 expressing the calcium indicator G-CaMP2.2b 47 in AWC^{ON} under the *str-2* promoter was crossed to *unc-2(lj1)* and *calf-1(ky867)* to generate the strains CX11391 and CX11386. For AIB imaging, the strain CX7469 expressing G-CaMP1.0 in AIB neurons 30 was crossed with *unc-2(lj1)* and *calf-1(ky867)* to generate CX11394 and CX11383. Animals were washed in buffer without food for ~20 minutes prior to imaging, a protocol designed to mimic the washes before chemotaxis assays, and imaging was conducted in a polydimethylsiloxane (PDMS) chamber in which an animal's nose was exposed to a stream of buffer that could be switched between odor-containing and odor-free solutions using an electronically gated valve. The standard stimulus protocol consisted of a 5-minute step pulse of the 10^{-4} dilution of odor in S-basal (without cholesterol) followed by odor removal. G-CaMP fluorescence intensity was measured for 10 seconds before and 50 seconds after the onset or offset of the odor stimulus; the same animals were imaged for odor onset and offset. 100% values were set by taking the average response from 1–4s in the trace. Controls and mutants were interleaved during imaging.

Subcellular localization in neurons and intestinal epithelial cells

For endoplasmic reticulum markers, cDNAs of *C. elegans* homologs of mammalian cytochrome P450, RAMP4 and cytochrome b5 (abbreviated as CP450 and cb5) were obtained using primers flanking the open reading frame C49C8.4, F59F4.2 and C31E10.729. For the Golgi marker, a cDNA fragment of *C. elegans* alpha-mannosidase II (ManII in the text, the first 82 amino acids sequences including signal sequence/TM-anchor domain) was amplified from F58H1.1 29, 48. cDNAs were fused to mCherry at their C termini.

Individual regions of CALF-1 were tested for endoplasmic reticulum localization by expressing GFP-tagged CALF-1 mutants in intestinal epithelial cells, which are larger than

HHMI Author Manuscript

HHMI Author Manuscript

HHMI Author Manuscript

neurons and easier to examine for subcellular protein localization. Full-length GFP-tagged CALF-1 colocalized with the endoplasmic reticulum marker CP450::mCherry in intestinal epithelial cells.

Heat shock experiments

Experiments with *hsp16.2::calf-1* were performed on young adult hermaphrodites. A 30°C heat shock was given for 3 hours. The plates were then incubated at 20°C for 2 hours for recovery before scoring GFP::UNC-2 localization and swimming behavior.

Photoconversion experiments

Dendra2::UNC-2 was expressed under *tag-168* pan-neuronal promoter in *calf-1(ky867);unc-2(lj1)* double mutant background; transgenic animals carrying *hsp16.2::calf-1* were crossed into the Dendra2::UNC-2 expressing animals. Prior to photoconversion, L4 larvae expressing Dendra2::UNC-2 were mounted on an agar pad.

The tail regions of individual animals were illuminated with UV light with a 63x Plan-Apochromat objective to achieve local photoconversion. Animals were recovered on agar plates with OP50, and a 30°C heat shock was given for 1 hour. The plates were then incubated at 20°C for 3 hours before scoring Dendra2::UNC-2 localization in the head region. The maximum fluorescence intensity of the photoconverted Dendra2::UNC-2 was quantified at the perinuclear region of a single image of best focus after background fluorescent intensity subtraction. Individual animals were mounted on agar pads in the same orientation before and after heat shock to allow the comparison of the same tail neurons.

Swimming assay

Individual young adult worms were transferred into a drop of M9 buffer on top of agar plate. After a 30 second recovery period, body bends were counted for 2 minutes.

Statistical Analysis

For fluorescent images and swimming assay, statistical analysis was performed using Student’s unpaired t-test, Bonferroni t-test or Dunnett’s test as appropriate. For AIB calcium imaging experiments, responses with an average value of zero were counted as failures, and the fraction of failures was compared for each genotype by Chi-squared test (a nonparametric method appropriate for non- normally distributed data). Consistent results were obtained in two independent blocks of experiments.

Supplementary Material

Refer to Web version on PubMed Central for supplementary material.

Acknowledgments

We thank S. Chalasani, T. Maniar, and P. McGrath for their insights and advice, A. Bendesky, E. Feinberg, G. Lee, B. Lesch, M. Tsunozaki, L. Winzenread for comments on the manuscript, L. Looger for G-CaMP2.2b, K. Shen for *mCherry::rab-3*, and the *Caenorhabditis* Genetic Center (CGC) and the National Bioresource Project for strains. This work was supported by the Howard Hughes Medical Institute. Y.S. was supported by the Nakajima

Foundation, and C.I.B. is an Investigator of the Howard Hughes Medical Institute. We dedicate this paper to Masanori Obayashi.

References

1. Catterall WA. Structure and regulation of voltage-gated Ca2+ channels. Annu Rev Cell Dev Biol. 2000; 16:521–55. [PubMed: 11031246]
2. Arikkath J, Campbell KP. Auxiliary subunits: essential components of the voltage-gated calcium channel complex. Curr Opin Neurobiol. 2003; 13:298–307. [PubMed: 12850214]
3. Bidaud I, Mezghrani A, Swayne LA, Monteil A, Lory P. Voltage-gated calcium channels in genetic diseases. Biochim Biophys Acta. 2006; 1763:1169–74. [PubMed: 17034879]
4. Jeziorski MC, Greenberg RM, Anderson PA. The molecular biology of invertebrate voltage-gated Ca(2+) channels. J Exp Biol. 2000; 203:841–56. [PubMed: 10667967]
5. Smith LA, et al. A *Drosophila* calcium channel alpha1 subunit gene maps to a genetic locus associated with behavioral and visual defects. J Neurosci. 1996; 16:7868–79. [PubMed: 8987815]
6. Brooks IM, Felling R, Kawasaki F, Ordway RW. Genetic analysis of a synaptic calcium channel in *Drosophila*: intragenic modifiers of a temperature-sensitive paralytic mutant of *cacophony*. Genetics. 2003; 164:163–71. [PubMed: 12750329]
7. Kawasaki F, Zou B, Xu X, Ordway RW. Active zone localization of presynaptic calcium channels encoded by the *cacophony* locus of *Drosophila*. J Neurosci. 2004; 24:282–5. [PubMed: 14715960]
8. Schafer WR, Kenyon CJ. A calcium-channel homologue required for adaptation to dopamine and serotonin in *Caenorhabditis elegans*. Nature. 1995; 375:73–8. [PubMed: 7723846]
9. Richmond JE, Weimer RM, Jorgensen EM. An open form of syntaxin bypasses the requirement for UNC-13 in vesicle priming. Nature. 2001; 412:338–41. [PubMed: 11460165]
10. Mathews EA, et al. Critical residues of the *Caenorhabditis elegans unc-2* voltage-gated calcium channel that affect behavioral and physiological properties. J Neurosci. 2003; 23:6537–45. [PubMed: 12878695]
11. Canti C, et al. The metal-ion-dependent adhesion site in the Von Willebrand factor-A domain of alpha2delta subunits is key to trafficking voltage-gated Ca2+ channels. Proc Natl Acad Sci U S A. 2005; 102:11230–5. [PubMed: 16061813]
12. Dickman DK, Kurshan PT, Schwarz TL. Mutations in a *Drosophila* alpha2delta voltage-gated calcium channel subunit reveal a crucial synaptic function. J Neurosci. 2008; 28:31–8. [PubMed: 18171920]
13. Ly CV, Yao CK, Verstreken P, Ohyama T, Bellen HJ. *straightjacket* is required for the synaptic stabilization of *cacophony*, a voltage-gated calcium channel alpha1 subunit. J Cell Biol. 2008; 181:157–70. [PubMed: 18391075]
14. Bichet D, et al. The I–II loop of the Ca2+ channel alpha1 subunit contains an endoplasmic reticulum retention signal antagonized by the beta subunit. Neuron. 2000; 25:177–90. [PubMed: 10707982]
15. Viard P, et al. PI3K promotes voltage-dependent calcium channel trafficking to the plasma membrane. Nat Neurosci. 2004; 7:939–46. [PubMed: 15311280]
16. Kittel RJ, et al. Bruchpilot promotes active zone assembly, Ca2+ channel clustering, and vesicle release. Science. 2006; 312:1051–4. [PubMed: 16614170]
17. Long AA, et al. Presynaptic calcium channel localization and calcium-dependent synaptic vesicle exocytosis regulated by the Fuseless protein. J Neurosci. 2008; 28:3668–82. [PubMed: 18385325]
18. Nishimune H, Sanes JR, Carlson SS. A synaptic laminin-calcium channel interaction organizes active zones in motor nerve terminals. Nature. 2004; 432:580–7. [PubMed: 15577901]
19. Butz S, Okamoto M, Sudhof TC. A tripartite protein complex with the potential to couple synaptic vesicle exocytosis to cell adhesion in brain. Cell. 1998; 94:773–82. [PubMed: 9753324]
20. Lai M, et al. A tctex1-Ca2+ channel complex for selective surface expression of Ca2+ channels in neurons. Nat Neurosci. 2005; 8:435–42. [PubMed: 15768038]
21. Patel MR, et al. Hierarchical assembly of presynaptic components in defined *C. elegans* synapses. Nat Neurosci. 2006; 9:1488–98. [PubMed: 17115039]

HHMI Author Manuscript HHMI Author Manuscript HHMI Author Manuscript

HHMI Author Manuscript HHMI Author Manuscript HHMI Author Manuscript

22. Crump JG, Zhen M, Jin Y, Bargmann CI. The SAD-1 kinase regulates presynaptic vesicle clustering and axon termination. Neuron. 2001; 29:115–29. [PubMed: 11182085]
23. Zhen M, Huang X, Bamber B, Jin Y. Regulation of presynaptic terminal organization by *C. elegans* RPM-1, a putative guanine nucleotide exchanger with a RING-H2 finger domain. Neuron. 2000; 26:331–43. [PubMed: 10839353]
24. Hallam SJ, Goncharov A, McEwen J, Baran R, Jin Y. SYD-1, a presynaptic protein with PDZ, C2 and rhoGAP-like domains, specifies axon identity in *C. elegans*. Nat Neurosci. 2002; 5:1137–46. [PubMed: 12379863]
25. Zhen M, Jin Y. The liprin protein SYD-2 regulates the differentiation of presynaptic termini in *C. elegans*. Nature. 1999; 401:371–5. [PubMed: 10517634]
26. Hall DH, Hedgecock EM. Kinesin-related gene *unc-104* is required for axonal transport of synaptic vesicles in *C. elegans*. Cell. 1991; 65:837–47. [PubMed: 1710172]
27. Frokjaer-Jensen C, et al. Effects of voltage-gated calcium channel subunit genes on calcium influx in cultured *C. elegans* mechanosensory neurons. J Neurobiol. 2006; 66:1125–39. [PubMed: 16838374]
28. Bauer Huang SL, et al. Left-right olfactory asymmetry results from antagonistic functions of voltage-activated calcium channels and the Raw repeat protein OLRN-1 in *C. elegans*. Neural Develop. 2007; 2:24.
29. Rolls MM, Hall DH, Victor M, Stelzer EH, Rapoport TA. Targeting of rough endoplasmic reticulum membrane proteins and ribosomes in invertebrate neurons. Mol Biol Cell. 2002; 13:1778–91. [PubMed: 12006669]
30. Chalasani SH, et al. Dissecting a circuit for olfactory behaviour in *Caenorhabditis elegans*. Nature. 2007; 450:63–70. [PubMed: 17972877]
31. Zerangue N, Schwappach B, Jan YN, Jan LY. A new ER trafficking signal regulates the subunit stoichiometry of plasma membrane K(ATP) channels. Neuron. 1999; 22:537–48. [PubMed: 10197533]
32. Schwappach B, Zerangue N, Jan YN, Jan LY. Molecular basis for K(ATP) assembly: transmembrane interactions mediate association of a K+ channel with an ABC transporter. Neuron. 2000; 26:155–67. [PubMed: 10798400]
33. Troemel ER, Sagasti A, Bargmann CI. Lateral signaling mediated by axon contact and calcium entry regulates asymmetric odorant receptor expression in *C. elegans*. Cell. 1999; 99:387–98. [PubMed: 10571181]
34. Mello C, Fire A. DNA transformation. Methods Cell Biol. 1995; 48:451–82. [PubMed: 8531738]
35. Chudakov DM, Lukyanov S, Lukyanov KA. Tracking intracellular protein movements using photoswitchable fluorescent proteins PS-CFP2 and Dendra2. Nat Protoc. 2007; 2:2024–32. [PubMed: 17703215]
36. Yeh E, et al. A putative cation channel, NCA-1, and a novel protein, UNC-80, transmit neuronal activity in *C. elegans*. PLoS Biol. 2008; 6:e55. [PubMed: 18336069]
37. Grunwald ME, Mellem JE, Strutz N, Maricq AV, Kaplan JM. Clathrin-mediated endocytosis is required for compensatory regulation of GLR-1 glutamate receptors after activity blockade. Proc Natl Acad Sci U S A. 2004; 101:3190–5. [PubMed: 14981253]
38. Schwappach B. An overview of trafficking and assembly of neurotransmitter receptors and ion channels (Review). Mol Membr Biol. 2008; 25:270–8. [PubMed: 18446613]
39. Hendrich J, et al. Pharmacological disruption of calcium channel trafficking by the alpha2delta ligand gabapentin. Proc Natl Acad Sci U S A. 2008; 105:3628–33. [PubMed: 18299583]
40. Herrmann JM, Malkus P, Schekman R. Out of the ER--outfitters, escorts and guides. Trends Cell Biol. 1999; 9:5–7. [PubMed: 10087610]
41. Fromme JC, Orci L, Schekman R. Coordination of COPII vesicle trafficking by Sec23. Trends Cell Biol. 2008; 18:330–6. [PubMed: 18534853]
42. Kota J, Ljungdahl PO. Specialized membrane-localized chaperones prevent aggregation of polytopic proteins in the ER. J Cell Biol. 2005; 168:79–88. [PubMed: 15623581]
43. Michelsen K, Yuan H, Schwappach B. Hide and run. Arginine-based endoplasmic-reticulum-sorting motifs in the assembly of heteromultimeric membrane proteins. EMBO Rep. 2005; 6:717–22. [PubMed: 16065065]

HHMI Author Manuscript

HHMI Author Manuscript

HHMI Author Manuscript

44. Schutze MP, Peterson PA, Jackson MR. An N-terminal double-arginine motif maintains type II membrane proteins in the endoplasmic reticulum. Embo J. 1994; 13:1696–705. [PubMed: 8157008]

45. Anderson P. Mutagenesis. Methods Cell Biol. 1995; 48:31–58. [PubMed: 8531732]

46. Wicks SR, Yeh RT, Gish WR, Waterston RH, Plasterk RH. Rapid gene mapping in *Caenorhabditis elegans* using a high density polymorphism map. Nat Genet. 2001; 28:160–4. [PubMed: 11381264]

47. Tallini YN, et al. Imaging cellular signals in the heart in vivo: Cardiac expression of the high-signal Ca2+ indicator GCaMP2. Proc Natl Acad Sci U S A. 2006; 103:4753–8. [PubMed: 16537386]

48. Chen CC, et al. RAB-10 is required for endocytic recycling in the *Caenorhabditis elegans* intestine. Mol Biol Cell. 2006; 17:1286–97. [PubMed: 16394106]

HHMI Author Manuscript

HHMI Author Manuscript

HHMI Author Manuscript

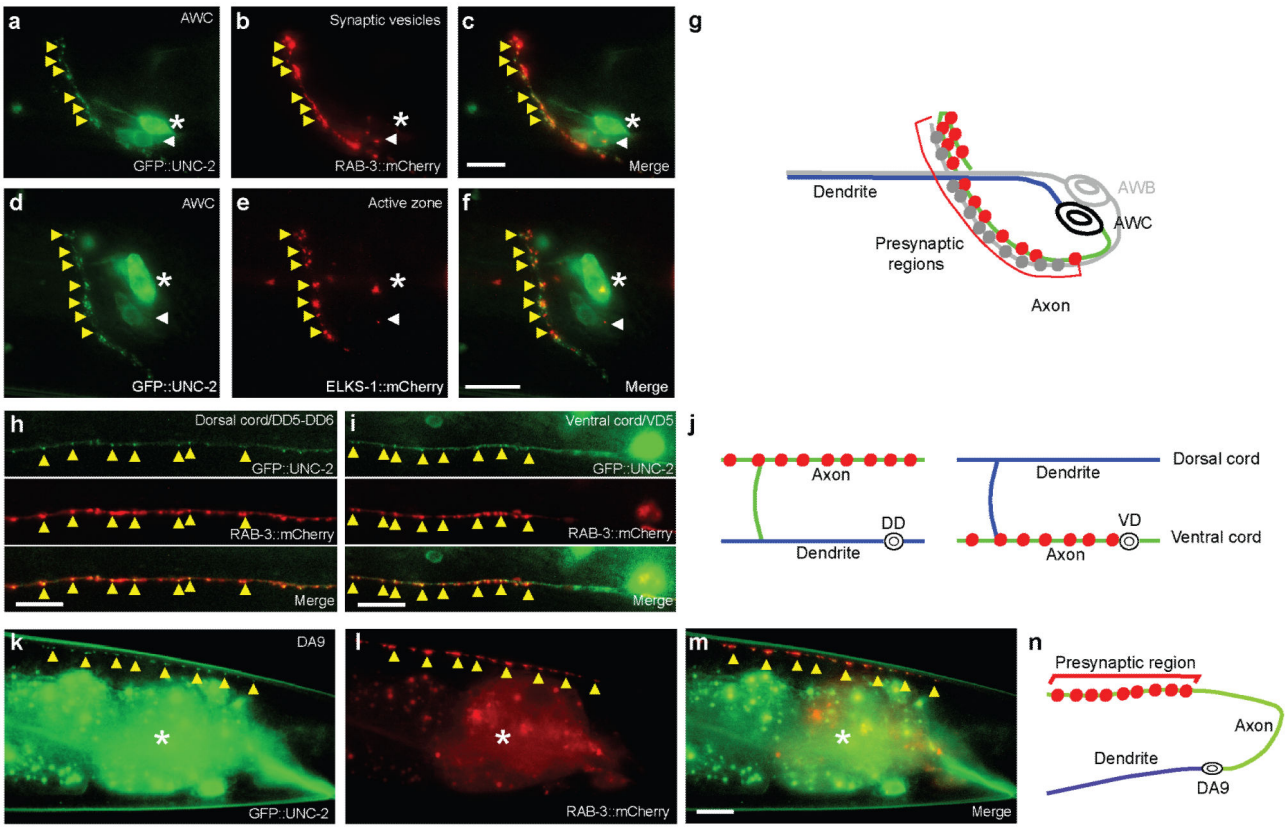

Figure 1. GFP-tagged UNC-2 localizes to presynaptic puncta in sensory neurons and motor neurons

(a–c) Representative images of GFP::UNC-2 and RAB-3::mCherry in the AWC cell body (white arrowhead) and axon (yellow arrowheads). The more dorsal cell body is AWB (asterisk). (d–f) Representative images of GFP::UNC-2 and ELKS-1::mCherry. (g) Schematic of AWC processes, with synapses in red. (h,i) Representative images of GFP::UNC-2 and RAB-3::mCherry in GABAergic motor neurons: DD axons (dorsal nerve cord) and VD axons (ventral nerve cord). (j) Schematic of VD and DD processes, with synapses in red. VD has a presynaptic region in its ventral process and DD has a presynaptic region in its dorsal process. (k–m) Representative images of GFP::UNC-2 and RAB-3::mCherry in the synaptic region of DA9 cholinergic neurons. The central autofluorescent region is the intestine (asterisk). (n) Schematic of DA9 processes. In all Figures, the AWC promoter is *odr-3*, which is also expressed weakly in AWB, ASH, AWA, and ADF sensory neurons; the VD/DD promoter is *unc-25;* the DA9 promoter is *itr-1;* and all data are taken from adult animals, unless otherwise noted. Head is to the left and dorsal is up in all images unless otherwise noted. Scale bar, 10 μm.

HHMI Author Manuscript

HHMI Author Manuscript

HHMI Author Manuscript

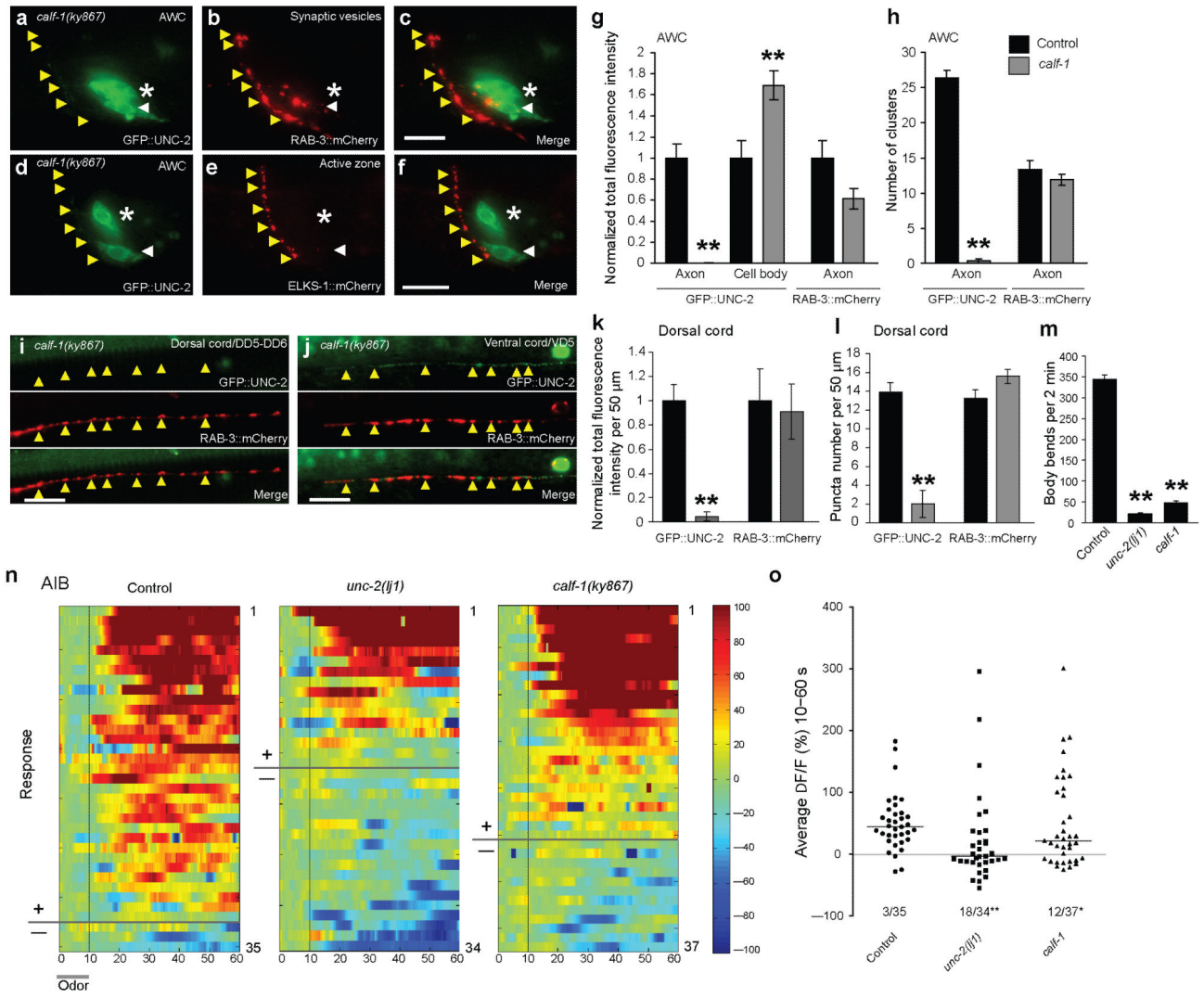

Figure 2. Presynaptic GFP::UNC-2 puncta are lost in *calf-1(ky867)* mutants

(a–c) Representative images of GFP::UNC-2 and RAB-3::mCherry in AWC neuron of a *calf-1(ky867)* mutant. (d–f) Representative images of GFP::UNC-2 and ELKS-1::mCherry in a *calf-1(ky867)* mutant. White arrowhead, AWC cell body; yellow arrowheads, AWC synapses; asterisk, AWB cell body. Compare Fig. 1a–f. (g, h) Quantification of GFP::UNC-2 and RAB-3::mCherry in AWC; (g) Normalized total fluorescence intensity and (h) number of fluorescent clusters. (i,j) Representative images of GFP::UNC-2 and RAB-3::mCherry in VD and DD neurons in a *calf-1(ky867)* mutant. Compare Fig. 1h,i. (k,l) Quantification of GFP::UNC-2 and RAB-3::mCherry in 50 µm covering DD5 and DD6 axons in the dorsal nerve cord; (k) Normalized total fluorescence intensity and (l) number of fluorescent puncta. Scale bar, 10 µm. (m) Quantification of swimming behavior in M9 buffer. All error bars indicate s.e.m. In g,h,k–m, asterisks indicate results different from wild-type controls by unpaired t-test at $P<0.01$ (**). (n) Calcium signals in AIB interneurons upon removal of the attractive odor isoamyl alcohol, which is sensed by AWC. Heat maps of individual recordings are shown for wild-type (n=35), *unc-2* (n=34), and *calf-1* (n=37)

adults. Odor was removed at t=10s. AWC responses and AIB odor-on responses are in Supplementary Figure 4. (o) Average AIB response to odor removal for traces shown in (n). Lines mark median response. Neurons with an average $\Delta F/F<0$ were scored as failures; both mutants were different from wild type in the fraction of failures, $P<0.05$ (*) or $P<0.01$ (**) by Chi-squared test.

HHMI Author Manuscript
HHMI Author Manuscript
HHMI Author Manuscript

HHMI Author Manuscript

HHMI Author Manuscript

HHMI Author Manuscript

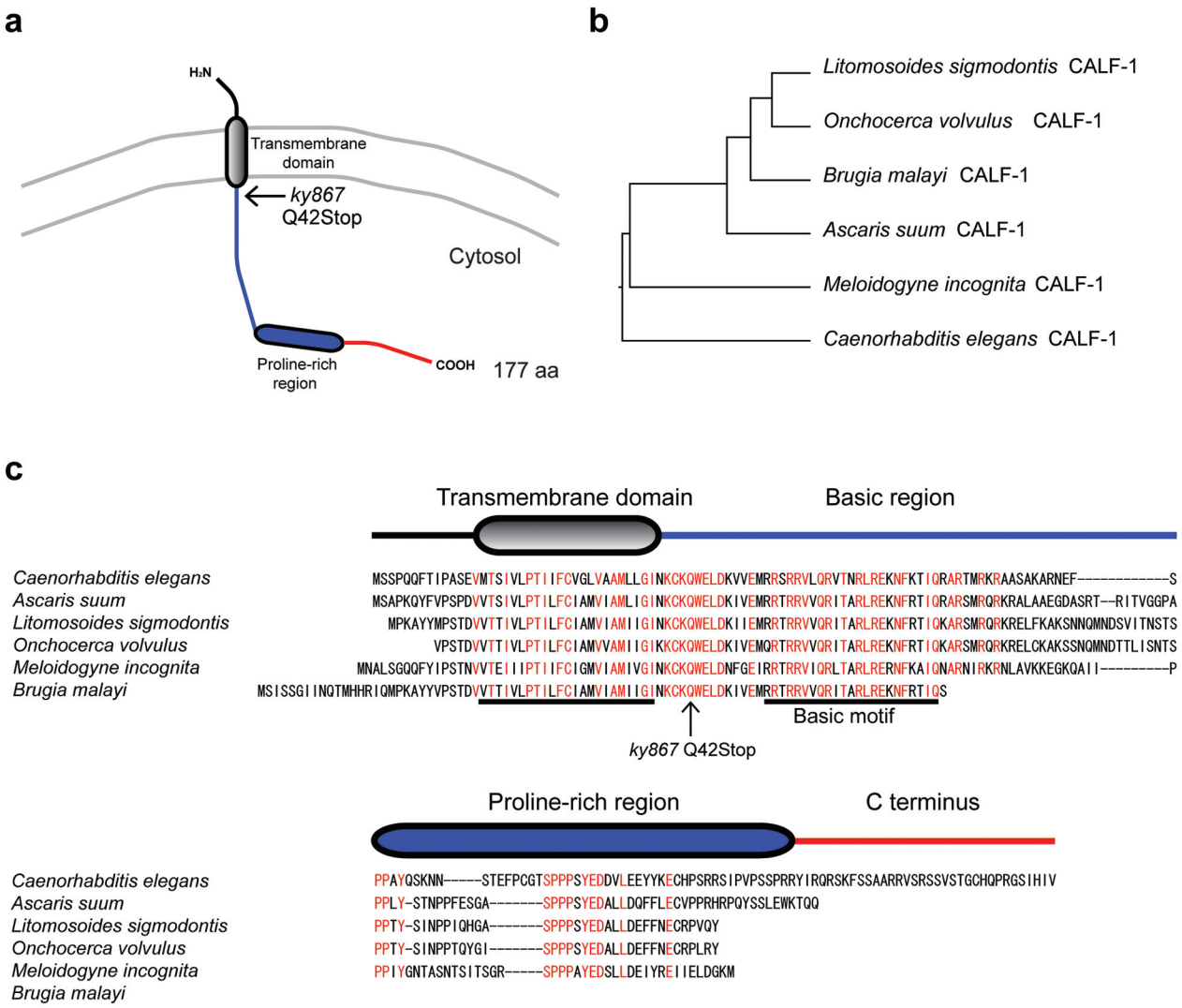

Figure 3. *calf-1* encodes a type I transmembrane protein

(a) A predicted topology of CALF-1, with a transmembrane domain near its N-terminus and basic and proline-rich regions in the predicted cytosolic region. The *ky867* allele has a termination codon after the transmembrane domain. (b) Phylogenetic tree of CALF-1 in nematodes. (c) Alignment of predicted nematode CALF-1 proteins. Invariant amino acids are in red.

HHMI Author Manuscript

HHMI Author Manuscript

HHMI Author Manuscript

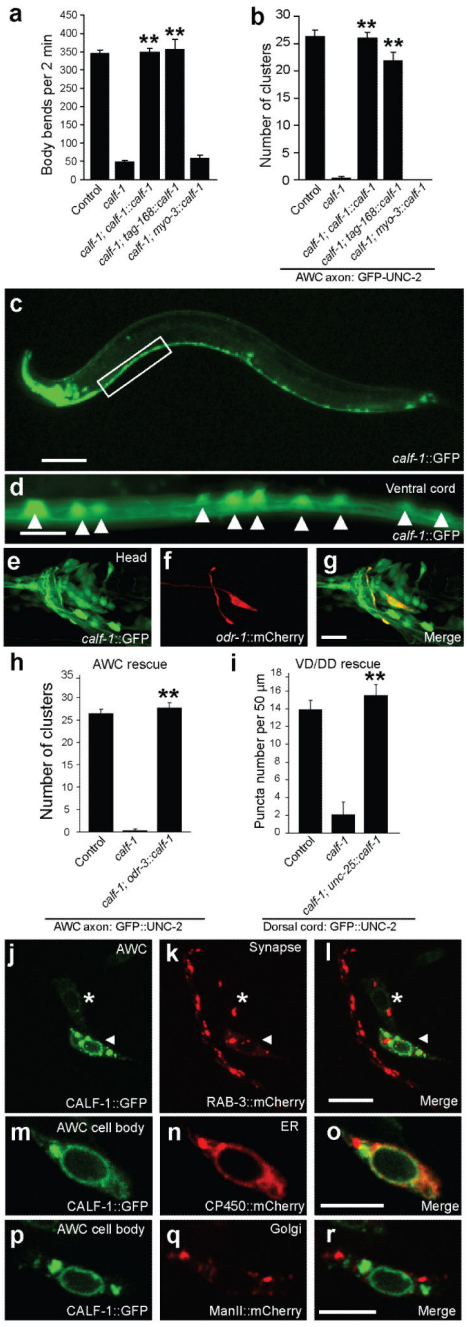

Figure 4. CALF-1 acts cell autonomously in neurons and localizes to endoplasmic reticulum

(a, b) Rescue of *calf-1(ky867)* mutants with *calf-1* cDNA under the endogenous *calf-1* promoter, pan-neuronal *tag-168* promoter, or muscle-specific *myo-3* promoter. (a) Swimming behavior in M9 buffer. (b) GFP::UNC-2 clusters in AWC axons. Asterisks denote strains different from *calf-1(ky867)* control by Bonferroni t-test, **= P<0.01. (c) Expression of *calf-1::GFP*, 0.8 kb of promoter sequence. Scale bar, 100 µm. (d) Boxed region from (c); motor neurons in the ventral nerve cord express *calf-1::GFP* (white arrowheads mark cell bodies). (e–g) AWC expresses *odr-1::mCherry* and *calf-1::GFP*. Scale bar, 10 µm. (h, i) Cell specific rescue of *calf-1(ky867)* mutants. (h) GFP::UNC-2

clusters in AWC axons, *odr-3::calf-1* rescue. (i) GFP::UNC-2 clusters in DD (dorsal cord), *unc-25::calf-1* rescue. Asterisks denote strains different from *calf-1(ky867)* controls at $P<0.01$ by unpaired t-test. All error bars indicate s.e.m. (j–l) Representative images of CALF-1::GFP and RAB-3::mCherry in AWC neurons. CALF-1::GFP is not visible at RAB-3-positive synapses. White arrowhead, AWC cell body; asterisk, AWB cell body. Scale bar, 10 μm. (m–r) Localization of CALF-1 in AWC cell body. (m–o) CALF-1::GFP and the endoplasmic reticulum (ER) marker CP450::mCherry in AWC. (p–r) CALF-1::GFP and the Golgi marker ManII::mCherry in AWC. Scale bar, 5 μm.

HHMI Author Manuscript
HHMI Author Manuscript
HHMI Author Manuscript

HHMI Author Manuscript
HHMI Author Manuscript
HHMI Author Manuscript

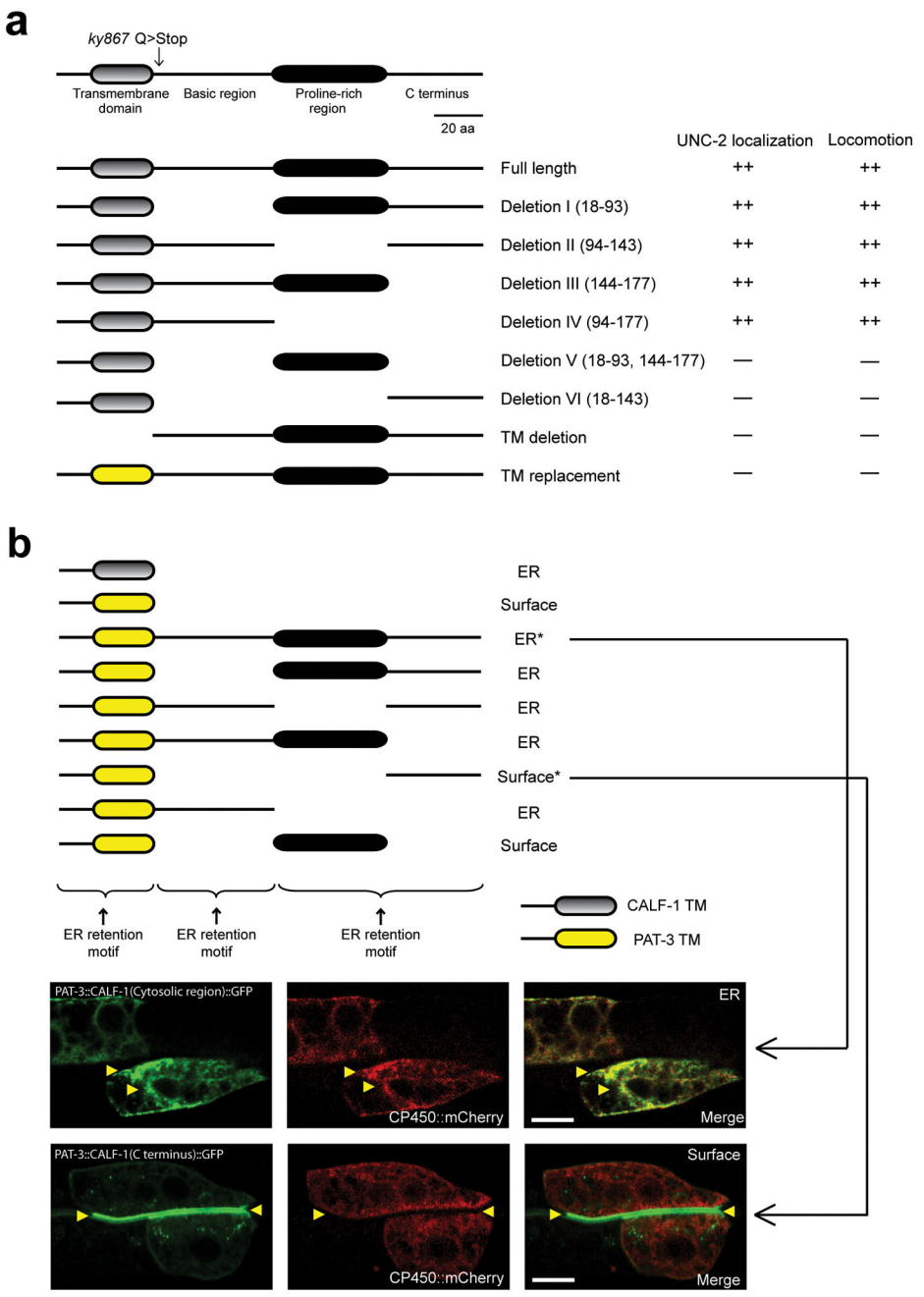

Figure 5. Structure-function analysis of CALF-1

(a) Schematic representation of CALF-1 and mutants tested for rescue. For AWC axon clusters, ++, >20 GFP::UNC-2 clusters per animal; —, <3 GFP::UNC-2 clusters (compare Fig. 2h). For locomotion, ++, >250 body bends/2 min; —, <100 body bends/2 min (compare Fig. 2m). (b) Distribution of endoplasmic reticulum (ER) retention motifs in CALF-1. Top, proteins tested by expression in intestinal epithelial cells. Bottom, plasma membrane and endoplasmic reticulum localization of representative fusion proteins in intestinal cells in L4 larva. Asterisks indicate sites of strong expression. Scale bar, 10 μm.

HHMI Author Manuscript HHMI Author Manuscript HHMI Author Manuscript

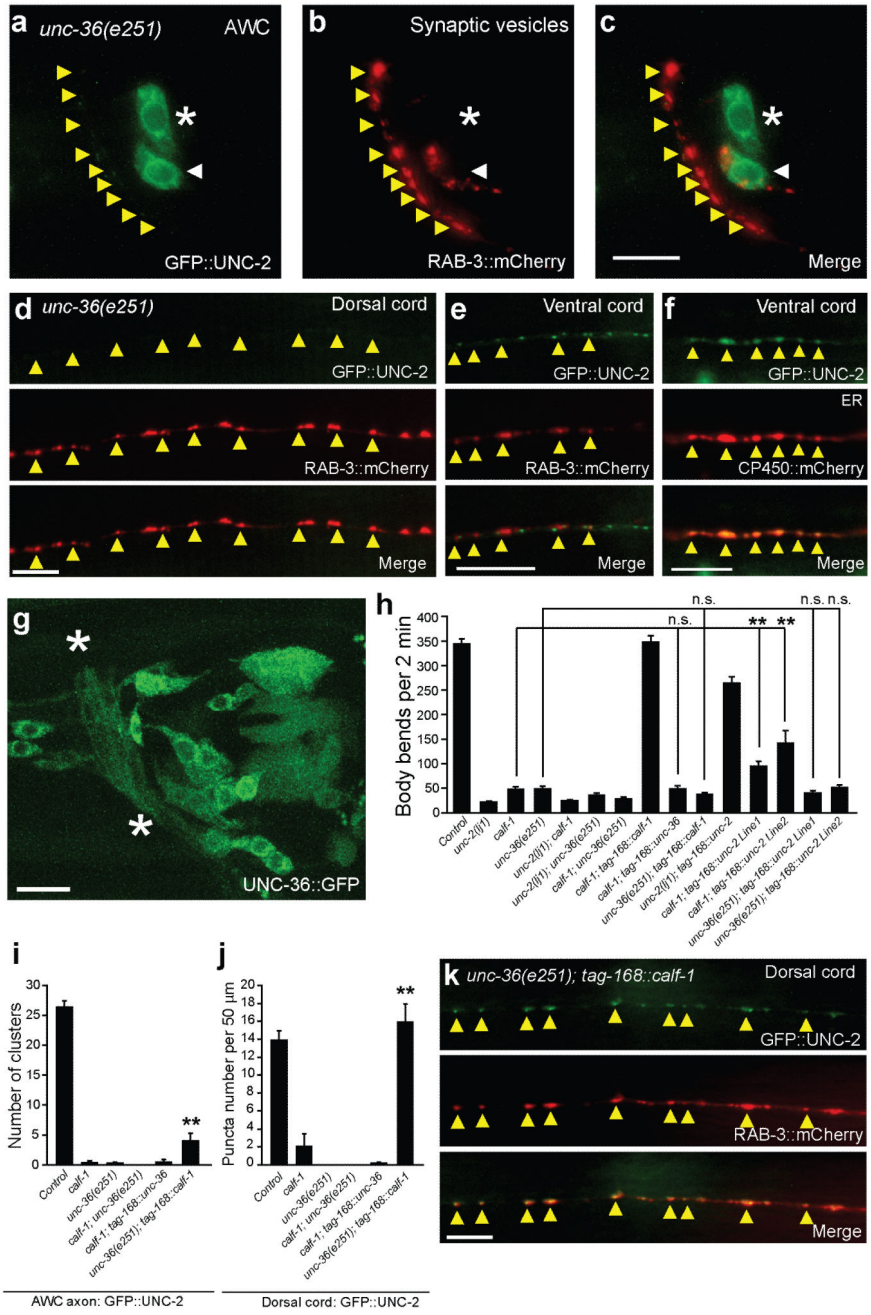

Figure 6. CALF-1 and UNC-36 have related trafficking functions

(a–c) GFP::UNC-2 and RAB-3::mCherry in AWC neuron of a *unc-36(e251)* mutant. White arrowhead, AWC cell body; yellow arrowheads, AWC synapses; asterisk, AWB cell body. (d) GFP::UNC-2 and RAB-3::mCherry in DD neurons of a *unc-36(e251)* mutant, dorsal nerve cord. (e) GFP::UNC-2 and RAB-3::mCherry in VD and DD neurons in a *unc-36(e251)* mutant, ventral nerve cord. (f) GFP::UNC-2 and the endoplasmic reticulum (ER) marker CP450::mCherry in VD and DD neurons in a *unc-36(e251)* mutant, ventral nerve cord. Compare Fig. 1a–i. (g) UNC-36::GFP expressed under the *unc-36* promoter, in the head of an adult; image analogous to panels a–c. Asterisks indicate diffuse localization

HHMI Author Manuscript

HHMI Author Manuscript

HHMI Author Manuscript

of UNC-36::GFP in axons at nerve ring. Scale bar, 10 μm. (h) Swimming behavior in M9 buffer. (i) GFP::UNC-2 clusters in AWC axons. (j) GFP::UNC-2 clusters in 50 μm of dorsal cord covering DD5 and DD6 axons. In h–j, asterisks denote results different from relevant single mutant strains at $P<0.01$ (**) by unpaired t-test or Bonferroni t-test, as appropriate; error bars indicate s.e.m. (k) GFP::UNC-2 and RAB-3::mCherry in DD neurons, dorsal nerve cord, of *unc-36(e251)* mutant overexpressing *tag-168::calf-1*.

HHMI Author Manuscript
HHMI Author Manuscript
HHMI Author Manuscript

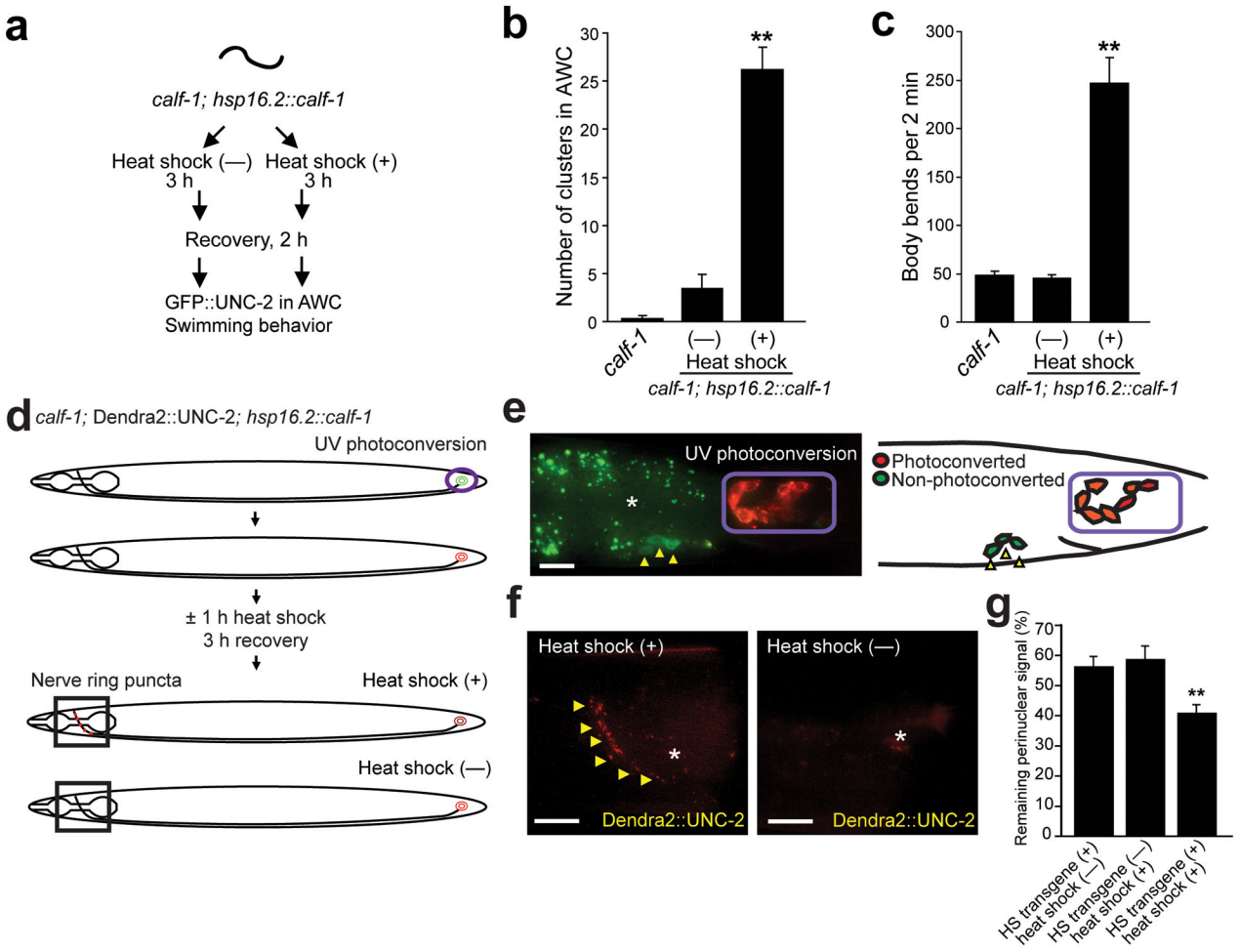

Figure 7. Acute CALF-1 expression transports UNC-2 from the cell body to the synapse

(a–c) Heat shock induction of *calf-1* rescues adult *calf-1(ky867)* mutants. (a) Schematic illustrating heat shock experiment. (b) GFP::UNC-2 puncta in AWC axons of heat-shocked and non-heat-shocked *calf-1; hsp16.2::calf-1* animals. (c) Swimming behavior in M9 buffer. (d) Schematic illustration of Dendra2::UNC-2 pulse-chase experiment. (e) Photoconverted Dendra2::UNC-2 in tail neurons; converted region circled in purple. Yellow arrowheads mark non-photoconverted cells. The central autofluorescence is from the intestine (asterisk). (f) Head region of heat-shocked animal and non-heat shocked animal. Arrowheads mark trafficked Dendra2::UNC-2 puncta at the nerve ring. Asterisks mark pharyngeal autofluorescence. (g) Photoconverted Dendra2::UNC-2 in the cell body. Asterisks denote results different from no heat shock controls at $P<0.01$ (**) by unpaired t-test. All error bars indicate s.e.m. Scale bar, 10μm.